



Double-blade structured triboelectric–electromagnetic hybrid generator with aerodynamic enhancement for breeze energy harvesting

Mingkang Zhu^{a,b,1}, Jiacheng Zhang^{b,1}, Zhaohui Wang^a, Xin Yu^b, Yuejun Zhang^c, Jianyang Zhu^{a,b,*}, Zhong Lin Wang^{b,d,*}, Tinghai Cheng^{b,*}

^a Key Laboratory of Metallurgical Equipment and Control Technology Ministry of Education, Wuhan University of Science and Technology, Wuhan, Hubei 430081, China

^b Beijing Institute of Nanoenergy and Nanosystems, Chinese Academy of Sciences, Beijing 101400, China

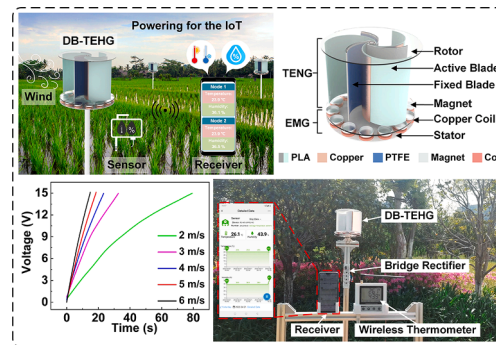
^c Institute of Circuits and Systems, Ningbo University, No.818 Fenghua Road, Ningbo 315211, China

^d School of Materials Science and Engineering, Georgia Institute of Technology, Atlanta, GA 30332-0245, United States

HIGHLIGHTS

- A double-blade structured triboelectric–electromagnetic hybrid generator is proposed.
- The double-blade structure can improve aerodynamic performance and can be used as a TENG unit.
- The DB-TEHG converts wind energy into electricity output with an efficiency of 20.88%.

GRAPHICAL ABSTRACT



ARTICLE INFO

Keywords:

Triboelectric nanogenerator
Triboelectric–electromagnetic hybrid generator
Breeze energy harvesting
Computational fluid dynamics simulation

ABSTRACT

Wind energy is a form of renewable energy with excellent development prospects. However, low-speed wind energy has not been effectively explored and utilized. To this end, a double-blade structured triboelectric–electromagnetic hybrid generator (DB-TEHG) is designed in this paper, which can efficiently harvest breeze energy by using double-blade structured design to improve the aerodynamic performance of the device. The improved blade structures directly drive the triboelectric nanogenerator (TENG) and electromagnetic generator (EMG) without requiring additional transmission systems. The blade parameters are simulated and optimized using computational fluid dynamics to enhance the wind energy harvesting capability of the device. The minimum starting wind speed of DB-TEHG is found to be 2 m/s. The output performance of a single TENG unit is 910 V, 45 μ A, 280 nC, and the peak power is 4 mW, and that of the EMG is 236 V, 24.2 mA, and a peak power of 0.5 W, when the wind speed is 5 m/s. It is also found that at this wind speed the DB-TEHG can convert wind energy into electricity output with an efficiency of 20.88%. The demonstration results prove that the proposed DB-TEHG can power a wireless thermometer by harvesting outdoor natural wind energy. This paper

* Corresponding authors.

E-mail addresses: zhujy@wust.edu.cn (J. Zhu), zhong.wang@mse.gatech.edu (Z.L. Wang), chengtinghai@binn.cas.cn (T. Cheng).

¹ These authors contributed equally to this work.

presents the application potential of DB-TEHG in the Internet of Things and also provides a novel solution to harvest breeze energy by combining TENGs and EMG.

1. Introduction

Developing renewable energy is effective for addressing the problem of energy shortage and for achieving carbon neutrality [1,2]. It is well-known that natural wind energy is a kind of sustainable energy with commercial development potential [3]. Existing applications of wind energy primarily involve the use of large vertical-axis wind turbines (VAWTs) [4]. Although such turbines exhibit high power generation capacities, they also have high wind speed requirements [5], which limit the harvesting of wind energy in areas with low-speed winds. Therefore, new technologies need to be developed to harvest and utilize low-frequency wind energy efficiently.

Wang's research group first proposed the triboelectric nanogenerator (TENG) in 2012 [6–10]. The TENG is based on the coupling effect of contact electrification and electrostatic induction [11–13], and it demonstrates advantages of a simple structure [14], low cost [15], high efficiency [16], wide selection of materials [17], and wide application scenarios [18]. Therefore, TENGs are widely used to harvest various forms of energy, including wave energy [19,20], wind energy [21–24], mechanical energy [25], and biomechanical energy [26] in the environment. Such applications of TENGs have demonstrated significant achievements and proven a few unique advantages in low-frequency energy harvesting [27].

According to existing research focused on TENGs, the devices employed to harvest wind energy primarily include the windmill type [28–29], flag-type [30], film flutter type [31], wind-induced swing type [32], as well as the most widely used wind cup type devices [33,34]. Due to the broadband characteristic of wind energy, the combination of TENG and electromagnetic generator (EMG) [35] is able to harvest wind energy effectively, and several studies have demonstrated the advantages of this hybrid mode [36,37]. However, to improve the performance of the generator, it is necessary to optimize the design of the energy harvesting device.

To efficiently harvest breeze energy, this paper proposes a novel double-blade structured triboelectric–electromagnetic hybrid generator (DB-TEHG), which is composed of three independent TENGs and an EMG. Based on the traditional VAWT, in the proposed DB-TEHG, a double-blade structured wind energy capture device is installed, which is optimized via computational fluid dynamics (CFD) simulations to obtain an appropriate combination of parameters. The novel double-blade design is capable of reducing wind drag during the upwind phase of the device operation, thereby the aerodynamic performance of the device is improved by increasing the drag difference between the downwind area and the upwind area, which enables the DB-TEHG to operate at a low wind speed of 2 m/s. Additionally, the double-blade structure can be employed as a TENG unit directly, and the DB-TEHG does not have any transmission system; thus, no extra energy is consumed. Further, in low-speed wind conditions, the TENG and the EMG operate together to improve the harvesting of breeze energy. Due to the double-blade structure, DB-TEHG can adapt to different wind speeds. The experimental results prove that the DB-TEHG can power a wireless thermometer after a period of operation when driven by outdoor natural wind. Thus, the results verify that the DB-TEHG can effectively harvest breeze energy and demonstrates good potential for engineering applications; hence, this creative design provides a new solution for harvesting and utilizing breeze energy.

2. Results and discussion

2.1. Structural design and operation principle

Because TENGs are able to transform breeze energy into electrical output, they can be used to supply power for various small sensors outdoors. As depicted in Fig. 1a, a DB-TEHG based on TENG and VAWT is used to power sensors to realize remote monitoring of farmland temperature and humidity, which envisages the application potential of the DB-TEHG to the Internet of Things (IoT). The DB-TEHG is made up of a rotor and a stator (Fig. 1b), and a prototype is presented in Fig. 1c. The rotor is composed of three pairs of blades, each of which includes an arched fixed blade and a semicircular active blade, as presented in Fig. 1d(i). Polytetrafluoroethylene (PTFE) is chosen as triboelectric material and copper as electrode material, because they have proved to be suitable materials for TENG [3]. A copper foil and a PTFE film are pasted on the fixed blade, and another copper foil is pasted on the active blade. In addition, the active blade can rotate about the edge of the fixed blade, which forms the contact–separation mode of the TENG. Three pairs of blades are evenly arranged in the middle of two acrylic plates with a diameter of 200 mm and rotate together around the central spindle. The back of the lower acrylic plate is fitted with 14 circular magnets with a diameter of 30 mm [Fig. 1d(ii)], and 14 copper coils of the same size are mounted onto the stator base [Fig. 1d(iii)], which forms the EMG.

As is the case with traditional drag-driven VAWT, when wind blows from any direction towards the DB-TEHG, the drag of the blade in the downwind area is greater than that in the upwind area (Fig. S1); this rotates the device. Further, the advantage of the double-blade structure is that the drag in the upwind area can be reduced while the drag in the downwind area can be maintained, which increases the drag difference across the device and improves the wind energy harvesting efficiency. Fig. 2a illustrates the working principle of the proposed DB-TEHG. The three pairs of blades are referred to as blade-1, blade-2, and blade-3, respectively. At the initial position [Fig. 2a(i)], under the action of wind, the active blade of blade-1 separates from the fixed blade; on the contrary, the active blade of blade-2 establishes contact with the fixed blade. As the device continues to turn, when the active blade of blade-1 crosses the upwind area [Fig. 2a(ii)], wind causes it to establish contact with the fixed blade of blade-1; simultaneously, the active blade of blade-3 begins to separate from the fixed blade under the force of wind. It is evident that each pair of blades completes a sequential transformation of the contact–separation state during this process, and this behavior is then repeated. A demonstration of the blade movement of the DB-TEHG can be found in Movie S1. In addition, the curved blade allows the TENG to possess a larger contact area compared with that of a flat structure.

With respect to the TENG, electricity generation is on the basis of the coupling effect of triboelectrification and electrostatic induction, and its principle in a complete cycle can be illustrated in three consecutive steps (Fig. 2b). Because the PTFE film is more electronegative than copper, when the blades are in contact [Fig. 2b(i)], electrons transfer from the copper-1 foil to the PTFE film; hence, positive charges accumulate on the surface of the former, and the latter possesses an equal number of negative charges. As the blades transition from a stage of contact to a stage of separation [Fig. 2b(ii)], a potential difference exists between them, which causes positive charges to transfer from copper-1 to copper-2 through the outside electric circuit, therefore generating a pulse current. Until the maximum distance between the electrodes is achieved, electrons accumulate on copper-2 [Fig. 2b(iii)]. Subsequently, as the device continues to rotate, the blades again come into contact, and the

induced electrons flow back owing to the absence of a potential difference, thereby generating a reverse current. Thus, with the continuous rotation of blades, the TENG can continuously generate periodic alternating current. The open-circuit voltage of a TENG (V_{OC}^{TENG}) is described by the following equation:

$$V_{OC}^{TENG} = -\frac{Q}{S\epsilon_0}(d_0 + x(t)) + \frac{\sigma x(t)}{\epsilon_0} \quad (1)$$

where Q denotes the transferred charges, S denotes the size of the contact area, ϵ_0 denotes the dielectric constant of vacuum, d_0 denotes the effective dielectric thickness, $x(t)$ denotes the real-time contact-separation distance, and σ denotes the triboelectric surface charge density. Furthermore, the short-circuit current of a TENG (I_{SC}^{TENG}) can be expressed as.

$$I_{SC}^{TENG} = \frac{2S\sigma d_0 x_{\max} f}{(d_0 + x(t))^2} \quad (2)$$

where x_{\max} denotes the maximum contact-separation distance, and f denotes the operating frequency of the TENG.

With respect to the EMG, electricity generation is according to Faraday's law of electromagnetic induction. As illustrated in Fig. 2c, when the rotor drives the magnet over the copper coil on the stator, continuous alternating current is generated due to the periodic change of magnetic flux through the coil. The open-circuit voltage and short-circuit current of the EMG (V_{OC}^{EMG} and I_{SC}^{EMG}) can be expressed as.

$$V_{OC}^{EMG} = -nN \frac{d\Phi}{dt} \quad (3)$$

$$I_{SC}^{EMG} = \frac{V_{OC}^{EMG}}{R_{coil}} \quad (4)$$

where n denotes the number of coils, N denotes the number of turns of the copper wire in a coil, Φ denotes the magnetic flux, and R_{coil} denotes the internal resistance of the copper coil.

2.2. CFD simulation and blade optimization

Based on Eqs. (1) and (2), it can be inferred that the size of the contact area (S) demonstrates a key impact upon TENG's output performance. Simultaneously, the blade size exerts an important influence on the wind-induced rotation of the device. Therefore, the blade size is a key research parameter. With the aim of improving the wind energy harvesting capacity of the DB-TEHG, the aerodynamic performance of the blades in an air flow field is analyzed via CFD simulations. More solution details about the numerical method are shown in Table S1.

First, a blade structure is designed, as illustrated in Fig. 3a(i), which involves cutting a rectangular hole on the surface of the blade of a traditional VAWT so that wind can pass through the hole and act on the active blade. The arc angle of the inner blade is α , and the arc angle of the hole is β . In addition, another design is presented in Fig. 3a(ii), which involves eliminating part of the blade of a traditional VAWT, and the arc angle of the retained part is θ . The parameters are illustrated in Fig. S2. For a preliminary comparison, set α , β , and θ to 80° . The active blade adopts a semicircular structure because the inside and outside of this shape are known to exhibit the highest drag difference, which aids in harvesting energy during the downwind phase and reducing drag during the upwind phase. Following this, the CFD method is used to simulate the performance of each model when the inlet velocity is 2 m/s. The direction of wind flow is from left to right, and the initial position is considered as the position at which the arched surface of blade-1 is facing the flow. The performance of the device is analyzed when it is rotated by 30° , 60° , and 90° from its initial position, and cloud images of the sectional pressure distribution at different angles of the model are captured, as illustrated in Fig. 3b(i) and Fig. 3b(ii). By comparing these two figures, it can be concluded that in the upwind phase, the end part of the fixed blade, illustrated in Fig. 3b(i), is evidently under pressure, which subjects blade rotation to a drag force. In the downwind phase, the shape of the fixed blade demonstrates no effect because the active blade bears all the pressure. Therefore, the model illustrated in Fig. 3a(ii) is expected to demonstrate better performance.

Second, the model illustrated in Fig. 3a(ii) is further simulated and optimized, and three contrast groups are set for θ . For groups A, B, and C, the corresponding values of θ are 80° , 90° , and 100° , respectively. The sectional pressure distribution cloud diagrams of each group are

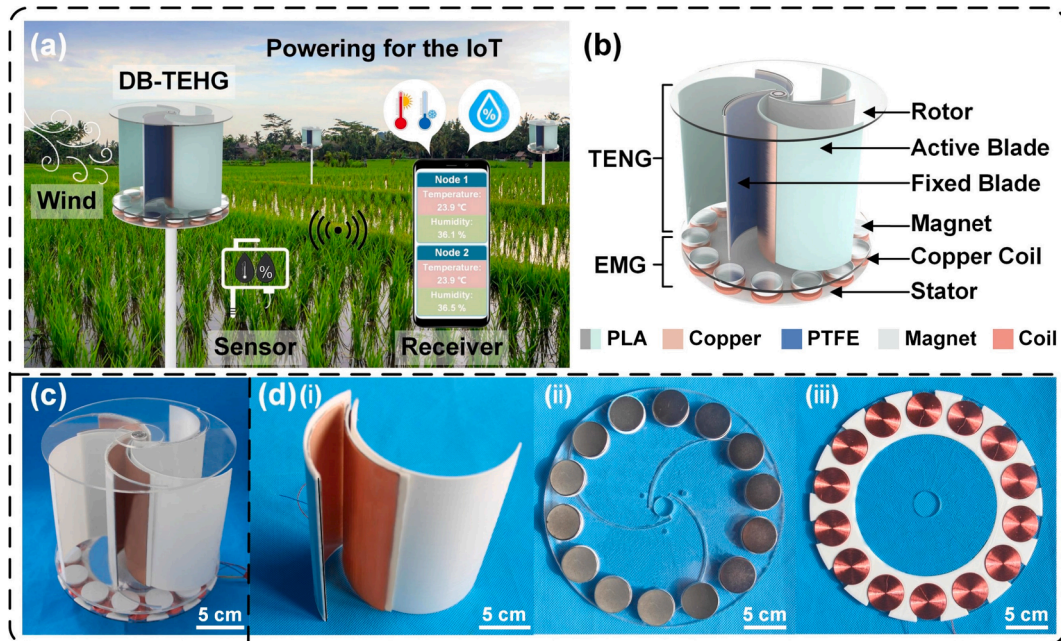


Fig. 1. Structural design of the DB-TEHG. (a) Application prospect of the DB-TEHG to sensor power supply in farmlands and IoT. (b) Schematic diagram of the DB-TEHG, (c) Photographs of the DB-TEHG device. (d) Photographs of components: (i) the blade and TENG unit; (ii-iii) rotor and stator of EMG.

recorded [Fig. 3b (ii-iv)], and from these distributions, it can be observed that the pressure is primarily distributed in the upwind area. A sectional velocity streamline diagram is presented in Fig. S3.

Furthermore, the torques of blade-1 and blade-2 and the overall torque of the device at each position are recorded (Fig. 3c). According to Fig. 3b and Fig. 3c, it can be concluded that blade-1 is subjected to a negative torque (T_1), i.e., the counterclockwise direction, which triggers its separation from the fixed blade. The torque of blade-2 (T_2) and that of the device (T) are positive, which trigger a smooth rotation of the device. For group A, T_2 and T performed best at 0° to 30° ; however, the performance degraded at 60° and 90° as the rotation position changed. Notably, the performance of group C is exactly opposite to that of group A. However, group B demonstrated the most balanced performance, with ideal performance over a rotational period. In contrast, although the torque of group B is smaller than that of group A at 0° and 30° , the size of the former is larger than that of the latter; hence, a larger sized electrode can be installed, which proves advantageous for the TENG. In addition, the aerodynamic differences between the improved and the traditional blades are analyzed via simulations, and the effects of different blade numbers on the improved device performance are compared, and the results are presented in Fig. S4 and Fig. S5. Therefore, after comprehensive analysis, group B is deemed to be the most appropriate, that is, when the arc angle (θ) of the fixed blade is 90° , the device exhibited the best aerodynamic performance.

2.3. Performance

To verify the above simulation results, an experimental test is con-

ducted on the DB-TEHG. Only one unit of the TENG is analyzed, as the three pairs of blades are installed in a rotationally symmetrical manner, and each unit is operated once during a rotational cycle. The output performances of groups A, B, and C when driven by different wind speeds are tested, and the output V_{OC}^{TENG} , I_{SC}^{TENG} , and Q_{SC} of a single TENG unit are obtained (Fig. 4).

The experimental results prove that the minimum starting wind speed of the DB-TEHG is 2 m/s, and the signal frequency of each group increases with the increase of wind speed, which implies that the rotational speed of the device gradually increased. However, when the wind speed is 5 m/s, the amplitude of the output signal of group C becomes zero. It is also discovered through the experiment that when the wind speed exceeds 5 m/s, the outputs of group A and group B also become zero. In other words, the TENG shuts down under this condition. This phenomenon can be attributed to the fact that as the rotational speed of the device increases, the rotational inertia of the active blade also increases; when the rotational inertia is greater than or equal to the torque generated by wind, the active blade is unable to separate from the fixed blade. From another perspective, when the rotational speed of the device increases, owing to the blockage effect [38], a lot of air flows around the device, and the wind pressure acting on the outer surface of the active blade is reduced, resulting in difficult separation of the active blade. As can be observed from Fig. S3, the wind speed around the device is higher, and this phenomenon appears more pronounced for group C, which results in a premature shutting down of the TENG in group C. Furthermore, the difference between the double-blade structure and the blade of a traditional drag-driven VAWT at high wind speed is compared via simulations (Fig. S7). Consequently, it is proved that the double-

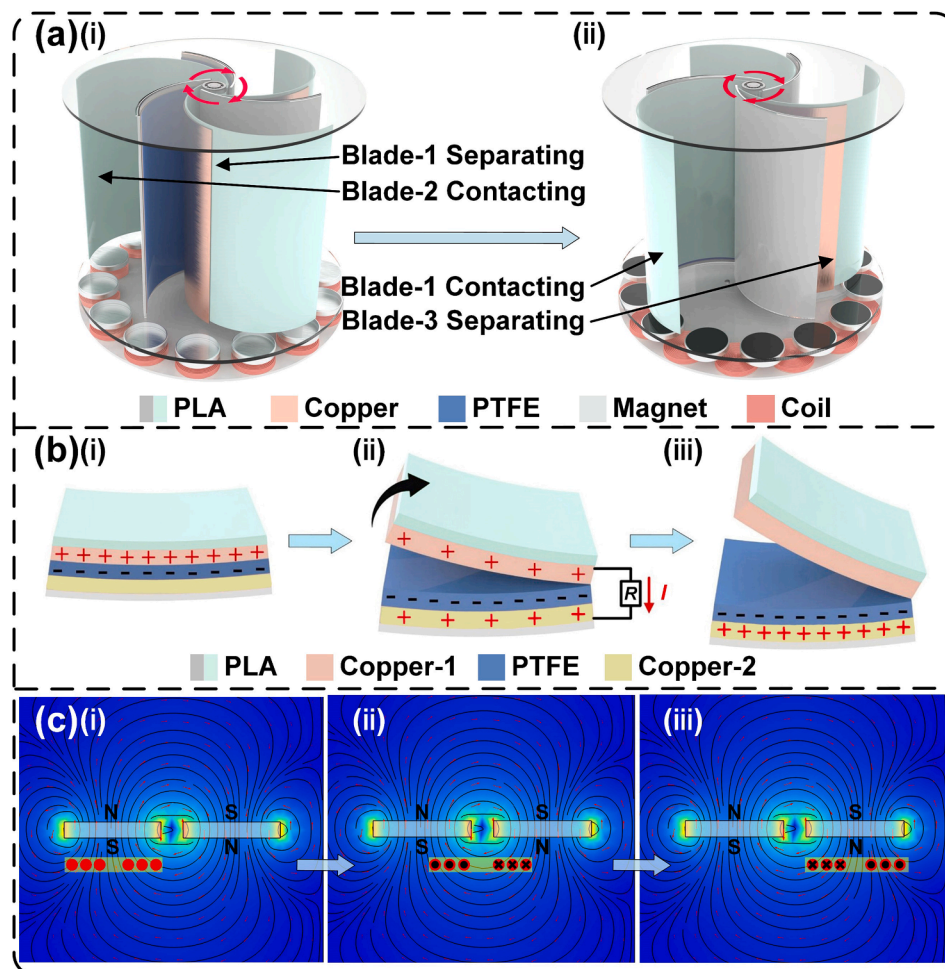


Fig. 2. Working principle of the DB-TEHG. (a) Working state of the blades at different stages. (b-c) Principle and charge transfer of the TENG and EMG.

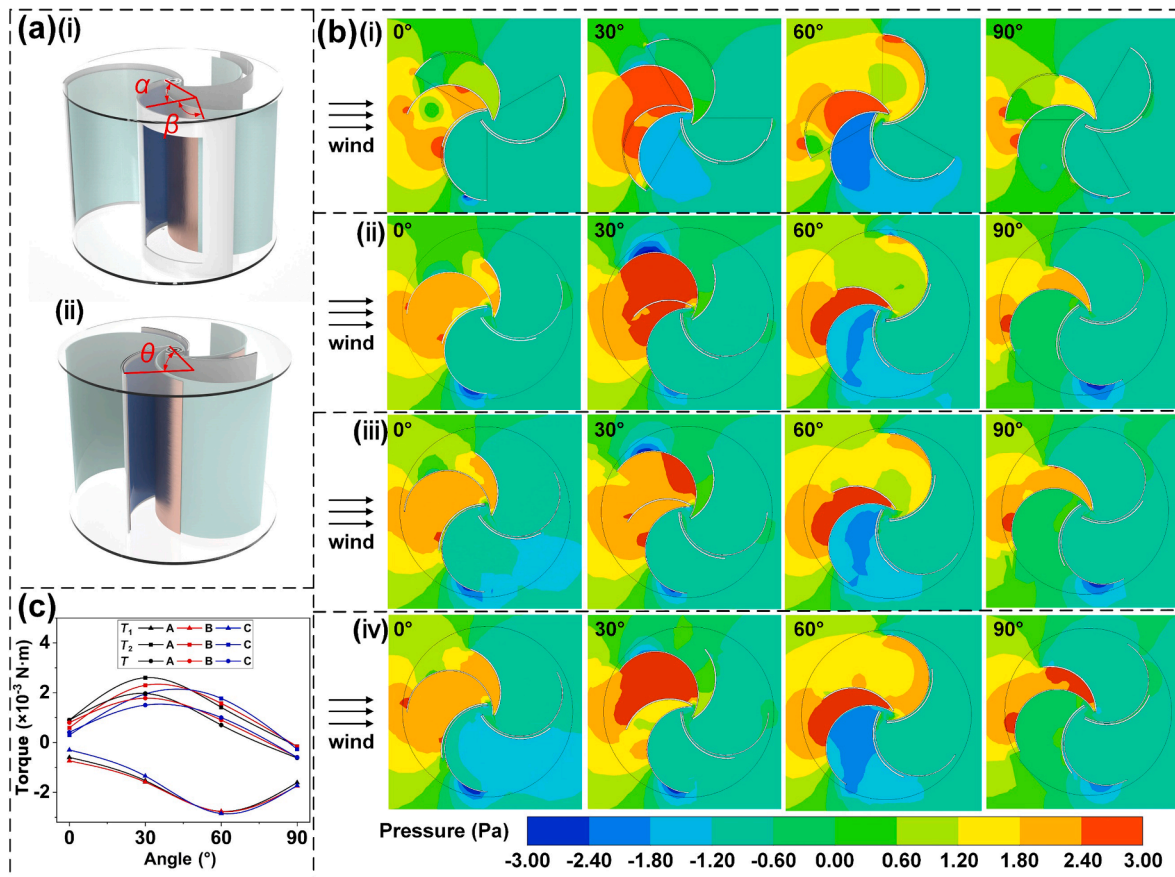


Fig. 3. Simulation and optimization of blades. (a) Structural design of the blade. (b) Sectional pressure distribution cloud diagrams for each group: (i) group of blades with a rectangular hole and (ii-iv) group A, group B, and group C. (c) Torque of each group.

blade structure can still increase the drag difference while maintaining contact.

Evidently, group B demonstrated the best output performance. On one hand, although the output signal of group A presented the same growth trend as that of group B, its V_{OC}^{TENG} , I_{SC}^{TENG} , and Q_{SC} values are all smaller than those of group B. However, on the other hand, notwithstanding the fact that the output of group C is approximately 3% higher than that of group B when the wind speed is 2 m/s to 4 m/s, group C presented no output at the wind speed of 5 m/s. As for group B, when the wind speed increases from 2 to 5 m/s, V_{OC}^{TENG} increases from 650 to 910 V, I_{SC}^{TENG} increases from 31 to 45 μ A, and Q_{SC} increases from 0.19 to 0.28 μ C.

According to Eq. (1) and Eq. (2), the larger the contact area, the larger the corresponding V_{OC}^{TENG} and I_{SC}^{TENG} . The blades of group C have the largest contact area, and have the largest voltage and current when the wind speed is less than 5 m/s, while the blades of group A are the opposite. Thus, it can be seen that the experimental measurement results of the influence of contact area change on the output performance of TENG are consistent with the theoretical equation.

Because the operation of an EMG is only related to the rotor speed, it will continue running at high rotational speeds. In order to study the influence of the number of magnets and copper coils upon the output characteristics of an EMG, the output voltage and current at different numbers are tested and compared (Fig. 5a). It can be observed that as the number of magnets and coils increases, the V_{OC}^{EMG} and I_{SC}^{EMG} gradually increase; hence, it can be concluded that a combination of 14 magnets and 14 coils appears to be the most appropriate. The output characteristics of the EMG in group B is tested at different wind speeds, and the results are displayed in Fig. 5b and Fig. 5c. As the wind speed increases from 2 to 5 m/s, V_{OC}^{EMG} increases from 80 to 236 V, I_{SC}^{EMG} improves from 10

to 24.2 mA, and the maximum values of V_{OC}^{EMG} and I_{SC}^{EMG} are 360 V and 37 mA, respectively, at a wind speed of 6 m/s. Meanwhile, Fig. 5d depicts the load voltage and current of the EMG under different load resistances. The load power of a TENG and an EMG are obtained by the following equation: $P = I^2R$. The result proves that the peak power of the EMG is 0.5 W at a 5 k Ω load resistance. In addition, to verify the advantages of the improved blades, the load power of a traditional VAWT of the same size is tested in the experiment (Fig. S8). Notably, the peak power of the EMG is 0.4 W. Therefore, the improved device can not only harvest more energy from the TENG but also improve the output power of the EMG by approximately 25%.

Fig. 5e illustrates the signal frequency of the TENG and EMG when the DB-TEHG is driven at different wind speeds. It proves that the TENG and the EMG operate together at a low wind speed of 2 to 5 m/s, and the operation of the DB-TEHG automatically switches to EMG-only operation when the wind speed exceeds 5 m/s. This avoids vibration caused by high-frequency contact and separation of the active blade. Thus, it can be concluded that the DB-TEHG can automatically adapt to different wind speed conditions. This not only improves the working range and energy capture efficiency of the device but also reduces the risk of damage caused to the device at high rotational speeds.

Furthermore, according to the frequency of signals, the rotational speeds of each group driven by different wind speeds can be obtained (Table S2), and the comparison and summary of the output performances of certain triboelectric–electromagnetic hybrid wind energy generators are shown in Table S3. The torques of the rotating shaft in each group at different wind speeds are measured by torque sensors (Fig. S9), the result proves that group B had the best performance, which is consistent with the simulation result.

According to the experimental data, when the wind speed is 5 m/s,

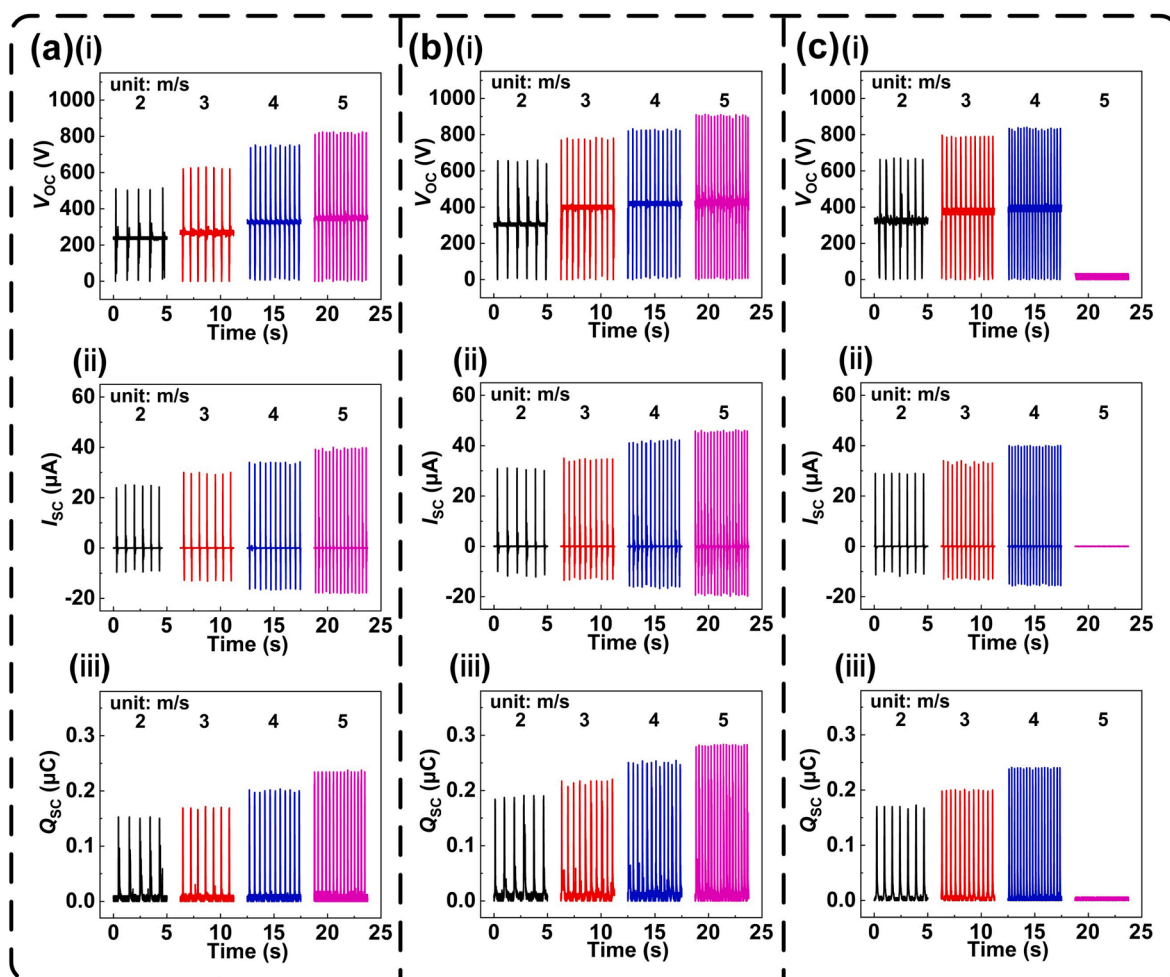


Fig. 4. Performance of the TENG unit of each group driven by different wind speeds. (a) Group A. (b) Group B. (c) Group C.

the efficiency of the DB-TEHG converting wind energy into mechanical energy is 23.36%, and the efficiency of the hybrid generator converting wind energy into electric energy output is 20.88%. Detailed derivation and calculation process are shown in Note S1.

2.4. Demonstration

A series of experiments are conducted by using a power management circuit (Fig. 6a) to demonstrate the actual output performance of the proposed DB-TEHG driven at 5 m/s wind speed. The load voltage and current of a TENG unit are measured under load resistances ranging from 0.2 M Ω to 3 G Ω [Fig. 6b(i)]. As the resistance increases, the voltage increases while the current decreases, and the peak power of the TENG unit is 4 mW when the load resistance is 10 M Ω . It can be obtained that the power density of the TENG is 0.38 W/m². Fig. 6b(ii) depicts the output power of the DB-TEHG at different wind speeds with a load resistance of 5 k Ω ; as can be observed, the peak power is 0.505 W at a wind speed of 5 m/s. Based on this, it can be concluded that the output performance of the DB-TEHG improves gradually as the wind speed increases. Moreover, Fig. S10 illustrates the time required to charge different commercial capacitors up to 5 V by employing three TENG units in parallel. As mentioned previously, the hybrid generator is formed by connecting a TENG and EMG in parallel, and Fig. 6c illustrates the time required to charge an 11 mF capacitor up to 15 V via the DB-TEHG at different wind speeds.

In addition, it is successfully demonstrated that each TENG unit is capable of supplying power to 120 blue light-emitting diodes (LEDs), and the EMG is capable of supplying power to 60 red LEDs (Fig. 6d and

Movie S2). Further, the results reveal that the three TENG units operate in rotation while the EMG functions steadily. In addition, when the wind speed exceeds 5 m/s, the EMG functions alone and can supply power to 120 red LEDs (Fig. S11).

Fig. 6e(i) demonstrates the test system utilized for the DB-TEHG. The DB-TEHG is driven by a fan. Charged by three TENG units in parallel for approximately 4 min, a 220 μ F capacitor reaches a voltage of 4.5 V. The capacitor is then used to power a commercial calculator successfully, and the normal operation of the calculator is demonstrated in Movie S3. As illustrated in Fig. 6e(ii), a wireless thermometer is powered by the DB-TEHG outdoors. Driven by the natural wind flowing in the field, the DB-TEHG can operate normally and charge the capacitor (TENG and EMG work in parallel). After the capacitor is charged for a certain period of time, the wireless thermometer can operate successfully using the capacitor power supply, and the receiver can collect temperature and humidity data from the wireless sensor (Movie S4). Thus, this application test demonstrates the superior application potential of the DB-TEHG for outdoor environmental monitoring and IoT applications.

3. Conclusions

In summary, this work proposed a novel DB-TEHG that can efficiently harvest breeze energy by using double-blade structured design. The CFD method is used to simulate and analyze the influence of different parameters of the double-blade structure. The result shows that compared with the traditional VAWT, the DB-TEHG with double-blade structure can improve the aerodynamic performance by reducing drag during the upwind phase, and it is most suitable when the fixed blade

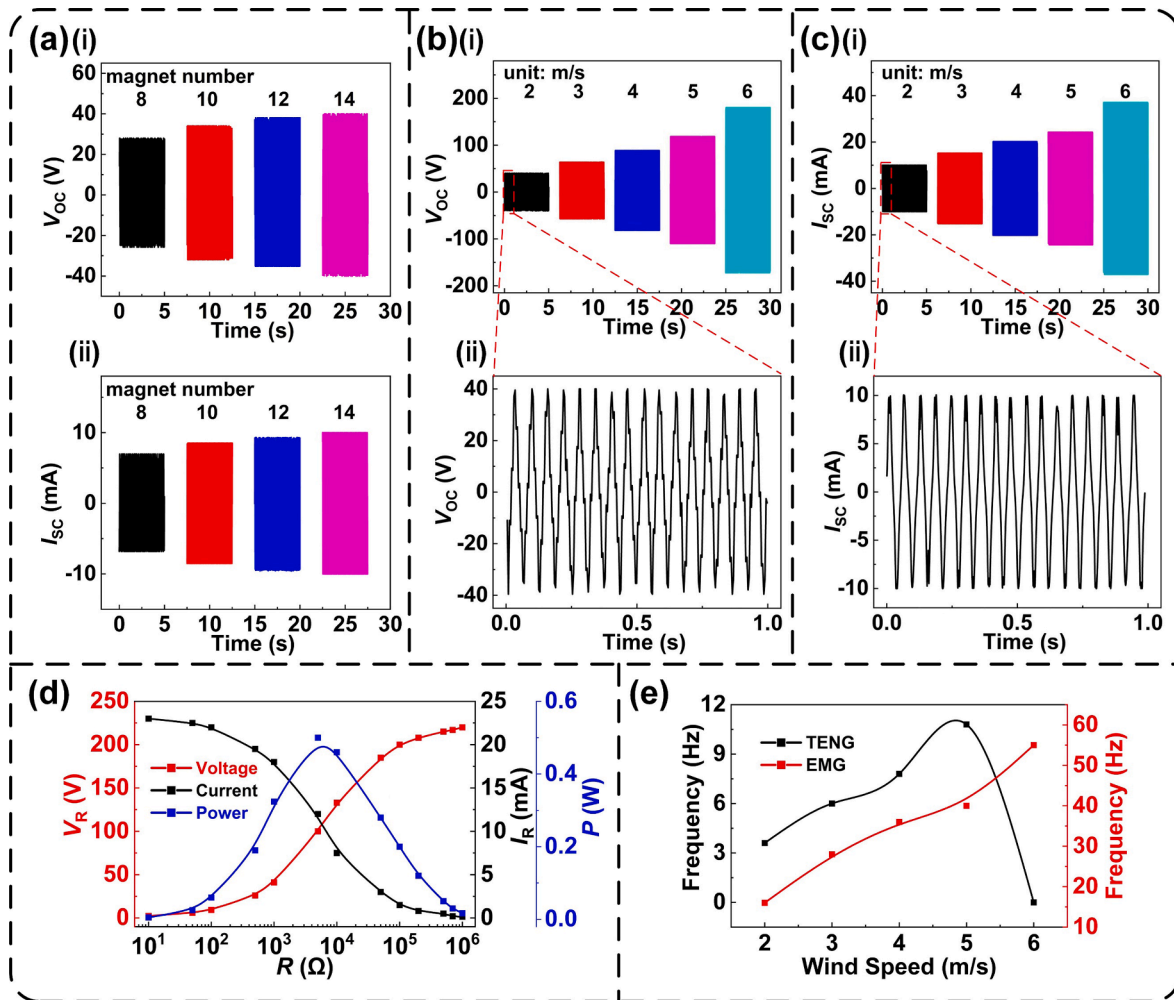


Fig. 5. Performance of an EMG unit. (a) Performance of the EMG with different magnet numbers driven at a wind speed of 2 m/s. (b-c) Performance of the EMG with 14 magnets driven at different wind speeds. (d) Effect of the load resistance on the output performance of the EMG. (e) Signal frequency of the TENG and the EMG when the DB-TEHG is driven at different wind speeds.

angle is 90° . Moreover, the accuracy of the simulation results is verified via experimental tests. The experimental results prove that the starting wind speed of the DB-TEHG is 2 m/s. At wind speed of 5 m/s, the maximum output open-circuit voltage and short-circuit current of a single TENG unit are 910 V and 45 μ A, and that of an EMG are 236 V and 24.2 mA. The efficiency of the DB-TEHG converting wind energy into electric energy output is 20.88%. Further, experiments prove that the DB-TEHG can power a wireless thermometer by harvesting outdoor natural wind energy. We believe that such a design provides a new solution for wind energy harvesting and utilization in windy environments and is expected to be used in IoT technologies and to power small sensors outdoors.

4. Experimental section

4.1. Fabrication of the DB-TEHG

The overall shape of the DB-TEHG is cylindrical, with a diameter of 200 mm and a height of 170 mm. The TENG consists of two 2 mm thick discs of acrylic material and three pairs of blades. The thickness of the blade is 1.5 mm, which is a three-dimensional structure printed using polylactic acid (PLA) material. The arc angle of the fixed blade is 90° , and the diameter is 110 mm, whereas the arc angle of the active blade is 180° , and the diameter is 100 mm. The dimensions of the copper electrode and PTFE film in the TENG unit are the following: length: 140 mm,

width: 75 mm, and thickness: 0.1 mm; the electrode and film have the same area of 105 cm^2 . For the EMG, the 14 magnets and 14 copper coils (diameter of the wire is 0.1 mm) used are of the same size, with a diameter of 30 mm and a thickness of 5 mm; they are placed with a spacing of 2 mm between them. In addition, adjacent magnets are placed with their N and S poles alternately facing upwards, and the coils are connected in series; they are evenly arranged on the back of the acrylic disk and the PLA base.

4.2. Electrical measurement

A fan is used as the wind source (FW-75A, AUX, China), and the wind speed is measured using a digital thermometer (AC826, SMART, China). The short-circuit current and transferred charge of the DB-TEHG are measured using a programmable electrometer (6514, Keithley, USA), and the data are recorded using a data acquisition system (USB-6211, National Instruments, USA). LabVIEW is used to process and display the data. The open-circuit voltage of the DB-TEHG is measured using an electron oscillograph (DS2202A, RIGOL, China).

CRediT authorship contribution statement

Mingkang Zhu: Conceptualization, Investigation, Writing – original draft. **Jiacheng Zhang:** Investigation, Writing – original draft, Validation. **Zhaohui Wang:** Investigation, Validation. **Xin Yu:** Validation. **Yuejun Zhang:** Investigation. **Jianyang Zhu:** Resources, Writing –

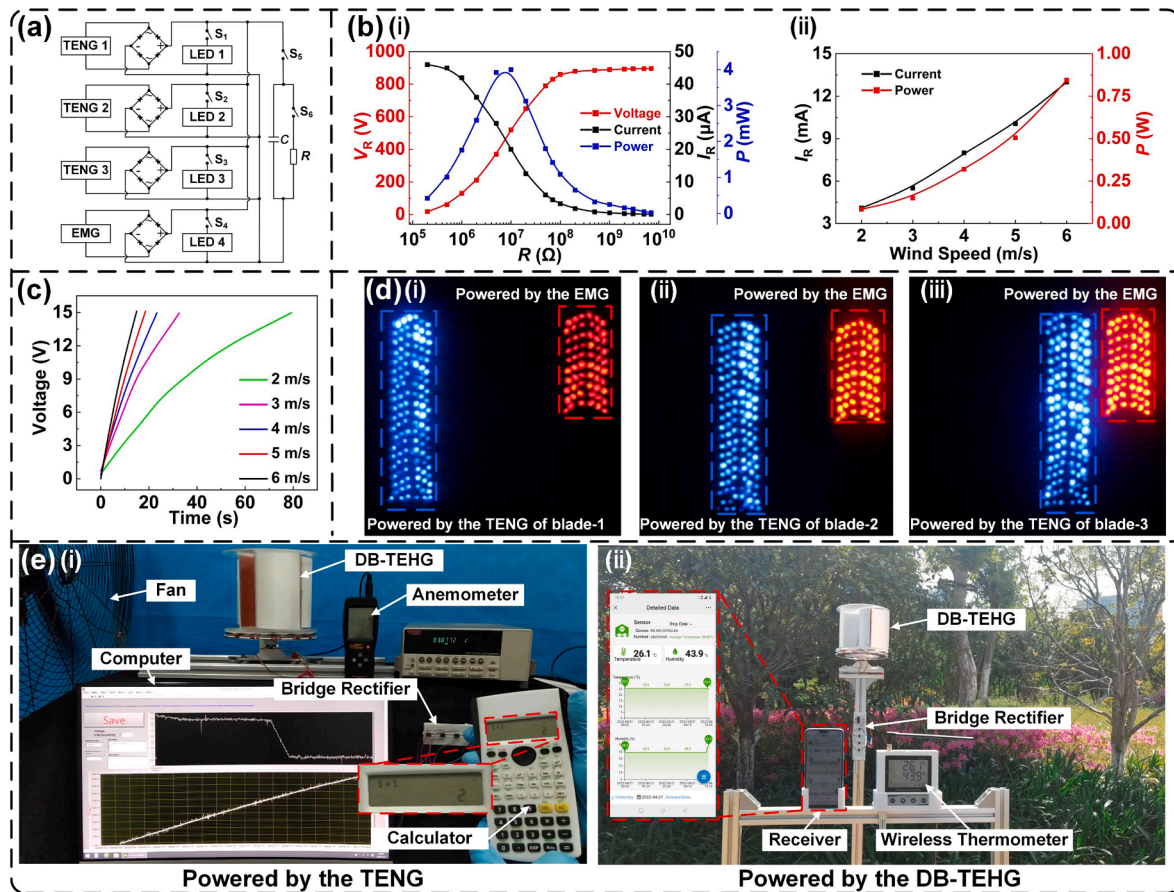


Fig. 6. Application demonstrations of the proposed DB-TEHG. (a) Power management circuit for the DB-TEHG. (b) Output performance of (i) the TENG with different load resistances and (ii) that of the DB-TEHG at different wind speeds. (c) Charging performance of the DB-TEHG for charging a capacitor at different wind speeds. (d) Photograph of the DB-TEHG powering 420 LEDs. (e) Test system: (i) a calculator powered using the TENG; (ii) wireless thermometer powered using the DB-TEHG outdoors.

review & editing, Supervision. **Zhong Lin Wang:** Conceptualization, Resources, Writing – review & editing, Supervision. **Tinghai Cheng:** Conceptualization, Resources, Writing – review & editing, Supervision.

Declaration of Competing Interest

The authors declare that they have no known competing financial interests or personal relationships that could have appeared to influence the work reported in this paper.

Data availability

Data will be made available on request.

Acknowledgements

The authors are grateful for the support received from the National Natural Science Foundation of China (project No. 51975429) and the Natural Science Foundation of Beijing Municipality (No. 3222023).

Appendix A. Supplementary material

Supplementary data to this article can be found online at <https://doi.org/10.1016/j.apenergy.2022.119970>.

References

- [1] Wang ZL, Jiang T, Xu L. Toward the blue energy dream by triboelectric nanogenerator networks. *Nano Energy* 2017;39:9–23. <https://doi.org/10.1016/j.nanoen.2017.06.035>.
- [2] Olabi AG, Abdelkareem MA. Renewable energy and climate change. *Renew Sust Energy Rev* 2022;158:112111. <https://doi.org/10.1016/j.rser.2022.112111>.
- [3] Chen B, Yang Y, Wang ZL. Scavenging wind energy by triboelectric nanogenerators. *Adv Energy Mater* 2018;8:1702649. <https://doi.org/10.1002/aenm.201702649>.
- [4] Porté-Agel F, Bastankhah M, Shamsoddin S. Wind-turbine and wind-farm flows: a review. *Boundary-Layer Meteorol* 2020;174:1–59. <https://doi.org/10.1007/s10546-019-00473-0>.
- [5] Ke W, Hashem I, Zhang W, Zhu B. Influence of leading-edge tubercles on the aerodynamic performance of a horizontal-axis wind turbine: a numerical study. *Energy* 2022;239:122186. <https://doi.org/10.1016/j.energy.2021.122186>.
- [6] Fan F-R, Tian Z, Wang ZL. Flexible triboelectric generator. *Nano Energy* 2012;1:328–34. <https://doi.org/10.1016/j.nanoen.2012.01.004>.
- [7] Wang ZL, Chen J, Lin L. Progress in triboelectric nanogenerators as new energy technology and self-powered sensors. *Energy Environ Sci* 2015;8:2250–82. <https://doi.org/10.1039/C5EE01532D>.
- [8] Zi Y, Guo H, Wen Z, Yeh M-H, Hu C, Wang ZL. Harvesting low-frequency (<5 Hz) irregular mechanical energy: a possible killer application of triboelectric nanogenerator. *ACS Nano* 2016;10:4797–805. <https://doi.org/10.1021/acsnano.6b01569>.
- [9] Wang ZL. On Maxwell's displacement current for energy and sensors: the origin of nanogenerators. *Mater Today* 2017;20:74–82. <https://doi.org/10.1016/j.mattod.2016.12.001>.
- [10] Cheng T, Gao Q, Wang ZL. The current development and future outlook of triboelectric nanogenerators: a survey of literature. *Adv Mater Technol* 2019;4:1–7. <https://doi.org/10.1002/admt.201800588>.
- [11] Wang ZL. On the expanded Maxwell's equations for moving charged media system – General theory, mathematical solutions and applications in TENG. *Mater Today* 2022;52:348–64. <https://doi.org/10.1016/j.mattod.2021.10.027>.

- [12] Wang ZL. Triboelectric nanogenerators as new energy technology and self-powered sensors – principles, problems and perspectives. *Faraday Discuss* 2014;176:447–58. <https://doi.org/10.1039/C4FD00159A>.
- [13] Wang ZL. From contact electrification to triboelectric nanogenerators. *Rep Prog Phys* 2021;84(9):096502. <https://doi.org/10.1088/1361-6633/ac0a50>.
- [14] Zhu G, Pan C, Guo W, Chen C-Y, Zhou Y, Yu R, et al. Triboelectric-generator-driven pulse electrodeposition for micropatterning. *Nano Lett* 2012;12(9):4960–5. <https://doi.org/10.1021/nl302560k>.
- [15] Chen P, An J, Shu S, Cheng R, Nie J, Jiang T, et al. Super-durable, low-wear, and high-performance fur-brush triboelectric nanogenerator for wind and water energy harvesting for smart agriculture. *Adv Energy Mater* 2021;11(9):2003066. <https://doi.org/10.1002/aenm.202003066>.
- [16] Li X, Zhang C, Gao Y, Zhao Z, Hu Y, Yang Ou, et al. A highly efficient constant-voltage triboelectric nanogenerator. *Energy Environ Sci* 2022;15(3):1334–45. <https://doi.org/10.1039/D1EE03961J>.
- [17] Dharmasena RDIG, Silva SRP. Towards optimized triboelectric nanogenerators. *Nano Energy* 2019;62:530–49. <https://doi.org/10.1016/j.nanoen.2019.05.057>.
- [18] Kim W-G, Kim D-W, Tcho I-W, Kim J-K, Kim M-S, Choi Y-K. Triboelectric nanogenerator: structure, mechanism, and applications. *ACS Nano* 2021;15:258–87. <https://doi.org/10.1021/acsnano.0c09803>.
- [19] Jing Z, Zhang J, Wang J, Zhu M, Wang X, Cheng T, et al. 3D fully-enclosed triboelectric nanogenerator with bionic fish-like structure for harvesting hydrokinetic energy. *Nano Res* 2022;15(6):5098–104. <https://doi.org/10.1007/s12274-022-4131-y>.
- [20] Wang A, Chen J, Wang Li, Han J, Su W, Li A, et al. Numerical analysis and experimental study of an ocean wave tetrahedral triboelectric nanogenerator. *Appl Energy* 2022;307:118174. <https://doi.org/10.1016/j.apenergy.2021.118174>.
- [21] He L, Zhang C, Zhang B, Yang Ou, Yuan W, Zhou L, et al. A dual-mode triboelectric nanogenerator for wind energy harvesting and self-powered wind speed monitoring. *ACS Nano* 2022;16(4):6244–54. <https://doi.org/10.1021/acsnano.1c11658>.
- [22] Li X, Cao Y, Yu X, Xu Y, Yang Y, Liu S, et al. Breeze-driven triboelectric nanogenerator for wind energy harvesting and application in smart agriculture. *Appl Energy* 2022;306:117977. <https://doi.org/10.1016/j.apenergy.2021.117977>.
- [23] Zhang B, Zhang S, Li W, Gao Qi, Zhao Da, Wang ZL, et al. Self-powered sensing for smart agriculture by electromagnetic–triboelectric hybrid generator. *ACS Nano* 2021;15(12):20278–86. <https://doi.org/10.1021/acsnano.1c08417>.
- [24] Liu Di, Chen B, An J, Li C, Liu G, Shao J, et al. Wind-driven self-powered wireless environmental sensors for Internet of Things at long distance. *Nano Energy* 2020;73:104819. <https://doi.org/10.1016/j.nanoen.2020.104819>.
- [25] Lu X, Li H, Zhang X, Gao B, Cheng T. Magnetic-assisted self-powered acceleration sensor for real-time monitoring vehicle operation and collision based on triboelectric nanogenerator. *Nano Energy* 2022;96:107094. <https://doi.org/10.1016/j.nanoen.2022.107094>.
- [26] Wang J, Jiang Z, Sun W, Xu X, Han Q, Chu F. Yoyo-ball inspired triboelectric nanogenerators for harvesting biomechanical energy. *Appl Energy* 2022;308:118322. <https://doi.org/10.1016/j.apenergy.2021.118322>.
- [27] Fu X, Bu T, Li C, Liu G, Zhang C. Overview of micro/nano-wind energy harvesters and sensors. *Nanoscale* 2020;12:23929–44. <https://doi.org/10.1039/D0NR06373H>.
- [28] Guo Y, Chen Y, Ma J, Zhu H, Cao X, Wang N, et al. Harvesting wind energy: A hybridized design of pinwheel by coupling triboelectrification and electromagnetic induction effects. *Nano Energy* 2019;60:641–8. <https://doi.org/10.1016/j.nanoen.2019.03.094>.
- [29] Fu X, Xu S, Gao Y, Zhang X, Liu G, Zhou H, et al. Breeze-wind-energy-powered autonomous wireless anemometer based on rolling contact-electrification. *ACS Energy Lett* 2021;6(6):2343–50. <https://doi.org/10.1021/acsenerylett.1c00704>.
- [30] Ye C, Dong K, An J, Yi J, Peng X, Ning C, et al. A triboelectric–electromagnetic hybrid nanogenerator with broadband working range for wind energy harvesting and a self-powered wind speed sensor. *ACS Energy Lett* 2021;6:1443–52. <https://doi.org/10.1021/acsenerylett.1c00244>.
- [31] Ren Z, Wang Z, Liu Z, Wang L, Guo H, Li L, et al. Energy harvesting from breeze wind (0.7–6 m s⁻¹) using ultra-stretchable triboelectric nanogenerator. *Adv Energy Mater*. 2020;10:2001770. <https://doi.org/10.1002/aenm.202001770>.
- [32] Zeng Q, Wu Y, Tang Q, Liu W, Wu J, Zhang Y, et al. A high-efficient breeze energy harvester utilizing a full-packaged triboelectric nanogenerator based on flow-induced vibration. *Nano Energy* 2020;70:104524. <https://doi.org/10.1016/j.nanoen.2020.104524>.
- [33] Yong S, Wang J, Yang L, Wang H, Luo H, Liao R, et al. Auto-switching self-powered system for efficient broad-band wind energy harvesting based on dual-rotation shaft triboelectric nanogenerator. *Adv Energy Mater* 2021;11(26):2101194. <https://doi.org/10.1002/aenm.202101194>.
- [34] Li X, Gao Q, Cao Y, Yang Y, Liu S, Wang ZL, et al. Optimization strategy of wind energy harvesting via triboelectric–electromagnetic flexible cooperation. *Appl Energy* 2022;307:118311. <https://doi.org/10.1016/j.apenergy.2021.118311>.
- [35] Zhang C, Tang W, Han C, Fan F, Wang ZL. Theoretical comparison, equivalent transformation, and conjunction operations of electromagnetic induction generator and triboelectric nanogenerator for harvesting mechanical energy. *Adv Mater* 2014;26:3580–91. <https://doi.org/10.1002/adma.201400207>.

- [36] Wen Z, Guo H, Zi Y, Yeh M-H, Wang X, Deng J, et al. Harvesting broad frequency band blue energy by a triboelectric–electromagnetic hybrid nanogenerator. *ACS Nano* 2016;10(7):6526–34. <https://doi.org/10.1021/acsnano.6b03293>.
- [37] Zhao J, Mu J, Cui H, He W, Zhang Le, He J, et al. Hybridized triboelectric–electromagnetic nanogenerator for wind energy harvesting to realize real-time power supply of sensor nodes. *Adv Mater Technol* 2021;6(4):2001022. <https://doi.org/10.1002/admt.202001022>.
- [38] Celik Y, Ma L, Ingham D, Pourkashanian M. Aerodynamic investigation of the start-up process of H-type vertical axis wind turbines using CFD. *J Wind Energy Ind Aerod* 2020;204:104252. <https://doi.org/10.1016/j.jweia.2020.104252>.



Mingkang Zhu received his M.S. degree from Wuhan University of Science and Technology in 2021. He is currently pursuing the Ph.D. degree at the same school, and is also a visiting student of Beijing Institute of Nanoenergy and Nanosystems, Chinese Academy of Sciences. His research interests are triboelectric nanogenerators and wind energy harvesters.



Jiacheng Zhang received his B.S. in School of Mechanical Engineering from Harbin University of Science and Technology, China, in 2018. He received his M.S. degree in School of Mechanical Engineering from Wuhan University of Science and Technology in 2021. He is currently a Ph.D. candidate in the same school. His research interests include fluid dynamics and fluid–structure interaction.



Dr. Zhaohui Wang received his B.S. and M.S. from Wuhan University of Science and Technology, China in 2003 and 2006 respectively, and received his Ph.D. from Chongqing University, China in 2009. He is currently a professor of Machinery and Automation at Wuhan University of Science and Technology in Wuhan, China. His research interests include computational fluid dynamics, heat and mass transfer, machinery design and optimization.



Dr. Xin Yu is a visiting scholar in Beijing Institute of Nanoenergy and Nanosystems, Chinese Academy of Sciences, currently. He obtained the B.S. and Ph.D. degrees from College of Electronic Science and Engineering, Jilin University in 2009 and 2014, respectively. He was a visiting scholar in Department of Electrical and Computer Engineering, Michigan State University from 2017 to 2018. His interests are triboelectric nanogenerators, infrared gas sensing, and photoelectric detection.



Dr. Yuejun Zhang received the Ph.D. degree in Communication and Information System from Ningbo University, China, in 2013. He is currently an associate professor in the Faculty of Electrical Engineering & Computer Science of Ningbo University. His research interests include hardware security, low power VLSI circuits and system, and memristor based neuromorphic computing.



Dr. Jianyang Zhu received his B.S. and M.S. degrees from Harbin Institute of Technology University, China in 2006 and 2008, respectively, and his Ph.D. in Fluid Machinery and Engineering in 2014. He is currently an assistant professor of Machinery and Automation at Wuhan University of Science and Technology in Wuhan, China. His research interests include fluid-structure interaction, fluid dynamics, and heat transfer.



Prof. Zhong Lin Wang received his Ph.D. from Arizona State University in physics. He now is the Hightower Chair in Materials Science and Engineering, Regents' Professor, Engineering Distinguished Professor and Director, Center for Nanostructure Characterization, at Georgia Tech. Dr. Wang has made original and innovative contributions to the synthesis, discovery, characterization and understanding of fundamental physical properties of oxide nanobelts and nanowires, as well as applications of nanowires in energy sciences, electronics, optoelectronics and biological science. His discovery and breakthroughs in developing nanogenerators established the principle and technological road map for harvesting mechanical energy from environment and biological systems for powering personal electronics. His research on self-powered nanosystems has inspired the worldwide effort in academia and industry for studying energy for micro-nano-systems, which is now a distinct disciplinary in energy research and future sensor networks. He coined and pioneered the field of piezotronics and piezophotonics by introducing piezoelectric potential gated charge transport process in fabricating new electronic and optoelectronic devices. Details can be found at: <http://www.nanoscience.gatech.edu>.



Prof. Tinghai Cheng received the B.S., M.S. and Ph.D. degrees from Harbin Institute of Technology in 2006, 2008 and 2013, respectively. He was a visiting scholar in the School of Materials Science and Engineering at Georgia Institute of Technology from 2017 to 2018. Currently, he is a professor of Beijing Institute of Nanoenergy and Nanosystems, Chinese Academy of Sciences, and CUSTech Institute of Technology (Wenzhou). His research interests are triboelectric nanogenerators, piezoelectric energy harvester, and piezoelectric actuators.